Enhanced Čerenkov second-harmonic emission in nonlinear photonic structures

K. Kalinowski,[1,*] P. Roedig,[2] Y. Sheng,[1] M. Ayoub,[2] J. Imbrock,[2] C. Denz,[2] and W. Krolikowski[1]

[1]*Laser Physics Center and Nonlinear Physics Center, Research School of Physics and Engineering, Australian National University, Canberra, ACT 0200, Australia*

[2]*Institute of Applied Physics and Center for Nonlinear Science (CeNoS), Westfälische Wilhelms-Universität Münster, Corrensstraße 2, 48149 Münster, Germany*

**Corresponding author: xkk124@physics.anu.edu.au*

Received February 8, 2012; accepted March 12, 2012;
posted March 14, 2012 (Doc. ID 162744); published May 18, 2012

We study experimentally and theoretically the Čerenkov-type second-harmonic generation in a one-dimensional nonlinear photonic crystal. We demonstrate that the power of emitted second-harmonic can be enhanced 270 times by varying the angle of incidence of the fundamental beam such that the reciprocal lattice vector of the crystal can be used to compensate for the phase mismatch in the transverse direction enabling interaction in the nonlinear Bragg diffraction regime.

OCIS codes: 190.0190, 190.2620, 190.4410, 190.4420.

Čerenkov second-harmonic generation (ČSHG) in nonlinear photonic crystals (NLPCs) with spatially modulated quadratic nonlinearity $\chi^{(2)}$ has attracted much attention recently [1–4]. From a fundamental point of view, the appearance of ČSHG is a result of light-matter interaction satisfying only the longitudinal (i.e., along propagation direction) phase-matching condition [5] [see Fig. 1(a)]. On the other hand, the efficient ČSHG is of great interest because of applications ranging from information technology to photobiology. For instance, the noncollinear propagation of the ČSHG with respect to the fundamental frequency (FF) may lead to remarkable improvement of signal-to-noise ratio in second-harmonic (SH) microscopy, so important for biological imaging and diagnostics of domain patterns in ferroelectric crystals [6].

It is of great practical importance to control the emission properties of the SH signals. For instance, it has been shown recently that one can vary the emission direction of ČSHG by either changing the angle of incidence of the fundamental beam [7] or by introducing modulation of nonlinearity in the longitudinal direction [8]. The frequency conversion can be also affected by the fundamental beam width and position [9], wavelength [10], and incidence angle [11–14]. The angular tuning of second-harmonic generation (SHG) in periodic structures is particularly interesting, as it enables one to use structures originally designed for a single wavelength in a much broader spectral range. Here we demonstrate that varying the angle of incidence of the fundamental wave leads to strong angular asymmetry and significant enhancement of the Čerenkov SH emission.

In the general case of NLPCs, the SH intensity I_2 is proportional to the square of the Fourier transform of the spatial modulation of nonlinearity with a phase mismatch wave vector $\mathbf{q}$ as a parameter [15]. For a one-dimensional (1D) structure with $\chi^{(2)}$ modulation in x direction, we get

$$I_2 = \frac{|E_1|^4 \omega^2 L_z^2 d_{\text{eff}}^2}{2c^3 \epsilon_0 L_x^2 n_2^2} |M(q_x)|^2 \text{sinc}^2\left(\frac{L_z q_z}{2}\right), \qquad (1)$$

where E_1, ω are the electric field and frequency of the fundamental wave, L_x, L_z are the lengths of the crystal in x and z directions, $d_{\text{eff}} = d_{31} \sin(\beta_2)$ is the effective nonlinear coefficient in our configuration, c is the speed of light, ϵ_0 is the permittivity of free space, n_2 is the refractive index at the SH, $q_x = k_2 \sin \beta_2 - 2k_1 \sin \beta_1$ and $q_z = k_2 \cos \beta_2 - 2k_1 \cos \beta_1$ are the phase mismatch vector components in x and z directions, and k_1, k_2 denote the wave vectors of the FF and the SH wave [see Fig. 1(b)]. $\beta_1(\alpha_1)$ and $\beta_2(\alpha_2)$ denote the incidence angle of the fundamental beam and the emission angle of SH inside (outside) the nonlinear medium with respect to c-axis. $|M(q_x)|^2$ is the square of the Fourier transform of the spatial modulation of the nonlinearity $\chi^{(2)}$ in x direction. In this paper, we assume that the nonlinear structure is not perfectly periodic with domain widths exhibiting a certain degree of randomness. In such a case, $|M(q_x)|^2$ must be replaced by its average $\langle |M(q_x)|^2 \rangle$ calculated over many domain distributions [16,17]. Since both q_x and q_z depend on the FF incident angle α_1 and the SH emission angle α_2, the SH intensity I_2 will be a function of both these angles. Figure 2 illustrates the mechanism of SH angle tuning in the form of color maps showing the contribution of q_z and q_x components of the phase mismatch $\mathbf{q}$ on SH intensity I_2. The graph in Fig. 2(a) depicts the term $sinc^2(L_z q_z/2)$ as a function of FF incidence angle α_1 and SH emission angle α_2. The maximum value of $sinc^2(L_z q_z/2)$ is 1, and it appears whenever $q_z = 0$ (i.e., $k_2 \cos \beta_2 = 2k_1 \cos \beta_1$). This is

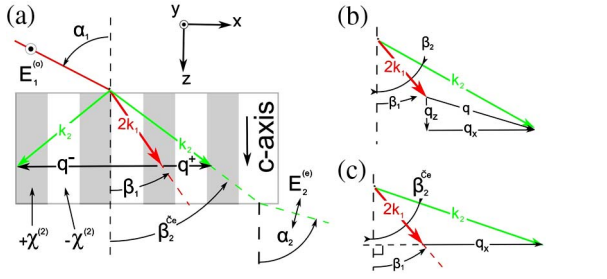

Fig. 1. (Color online) (a) The concept of Čerenkov SH in one-dimensional NLPCs. White and gray colors represent oppositely oriented ferroelectric domains. (b) and (c) Phase-matching diagram for general (b) and Čerenkov (c) SH process.

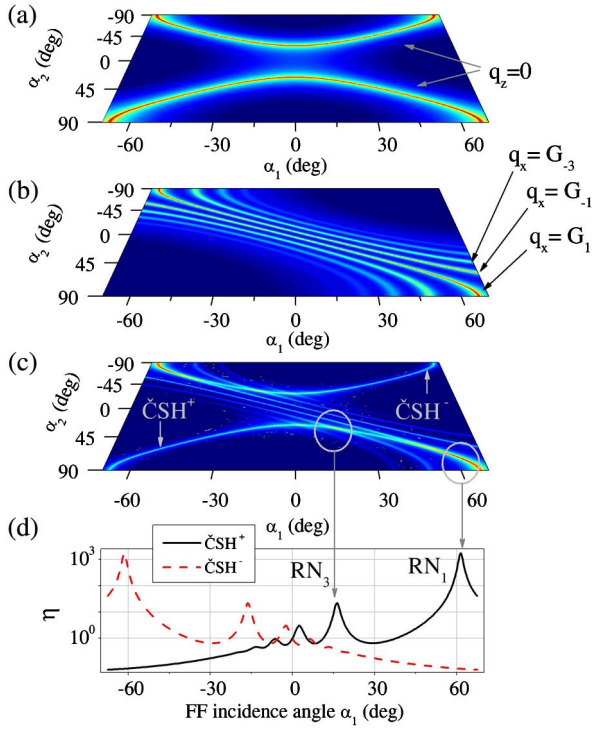

Fig. 2. (Color online) (a)–(c) Color map sequence showing the origin of Čerenkov SH radiation (color coding in logarithmic sale and adjusted arbitrary to emphasize key features). (d) Čerenkov SH enhancement profiles along $\check{C}SH^{+}$ and $\check{C}SH^{-}$ as indicated in (c).

exactly the Čerenkov condition, and it appears in the figure as two symmetric (with respect to $\alpha_1 = 0$ and $\alpha_2 = 0$) arches. Figure 2(b) depicts the term $\langle |M(q_x)|^2 \rangle$, which, in general, will depend on the structure of the nonlinearity $\chi^{(2)}$. Here we assumed that in our 1D structure, the domain width is described by Gamma distribution with dispersion $\sigma = 0.4\ \mu$m and mode (the most likely value) $l_m = 4.5\ \mu$m. The visible traces of high values appear where the process is transversely phase matched; i.e., q_x is equal to one of the reciprocal lattice vectors (RLV) $G_m = m2\pi/\Lambda$ (i.e., $k_2 \sin\beta_2 - 2k_1 \sin\beta_1 = G_m$), which is the so-called nonlinear Raman–Nath condition [2,7]. Since I_2 is the product of the terms shown in Figs. 2(a) and 2(b), the strong SHG can be expected when both Čerenkov ($q_z = 0$) and RN conditions ($q_x = G_m$) simultaneously fulfill what is known as a nonlinear Bragg diffraction [2]. This effect of efficient SHG is clearly visible if we plot ČSH enhancement defined as $\eta = I_2(\alpha_1)/I_2(\alpha_1 = 0)$ as a function of α_1. In Fig. 2(d), the dashed and solid lines show the ČSH enhancement profiles along $\check{C}SH^{-}$ and $\check{C}SH^{+}$, as marked in Fig. 2(c), respectively. For guidance, we marked two peaks resulting from Raman–Nath resonances as RN_1 and RN_3. It is clear that by manipulating the incidence angle α_1, one can achieve few orders of magnitude enhancement of one of the ČSH signals, and at the same time significant suppression of the other one.

In the experiment, we used a 500 μm-thick 1D poled lithium niobate sample with a nominal poling period of $\Lambda = 9\ \mu$m and duty cycle of 50%. The laser beam of 200 fs pulses at $\lambda = 1.50\ \mu$m, average power of 4.2 mW, and repetition rate of 952 Hz was collimated at the sample to the beam full width half maximum FWHM = 400 μm. The ordinary polarized fundamental beam was incident on the sample at the angle α_1 and propagated in the plane parallel to crystal optical c-axis [x-z plane in Fig. 1(a)]. The sample was mounted on a rotation stage that allowed us to control the incident angle. The generated SH was emitted at the angle α_2. The SH intensity was detected by the silicon photo diode mounted on the rotation stage, which allowed us to record the angular characteristics of the SH emission. We observe two couples of orthogonally polarized Čerenkov spots that originate via the OO-E and OO-O interactions. For the sake of clarity, we only discuss here the extraordinary component of the SH. However, our discussion is also valid for an ordinary component.

Figure 3(a) shows the measured SH enhancement as a function of fundamental wave incidence angle α_1 and SH emission angle α_2 (color in logarithmic scale). The two strongest curves located symmetrically with respect to $\alpha_2 = 0°$ represent the Čerenkov signals (labeled as $\check{C}SH^{+}$ and $\check{C}SH^{-}$). The numerous straight lines represent the weak Raman–Nath emission. The two strongest traces are RN_1 and RN_{-1} and are visible for all angles α_1. The remaining higher order RNs are visible only in the vicinity of the Čerenkov signal [e.g., $RN_{3,4,5}$ in Fig. 3(b)]. From Figs. 3(b) and 3(c), one can also see that the Čerenkov signal increases dramatically whenever the corresponding emission curve intersects with one of the emission

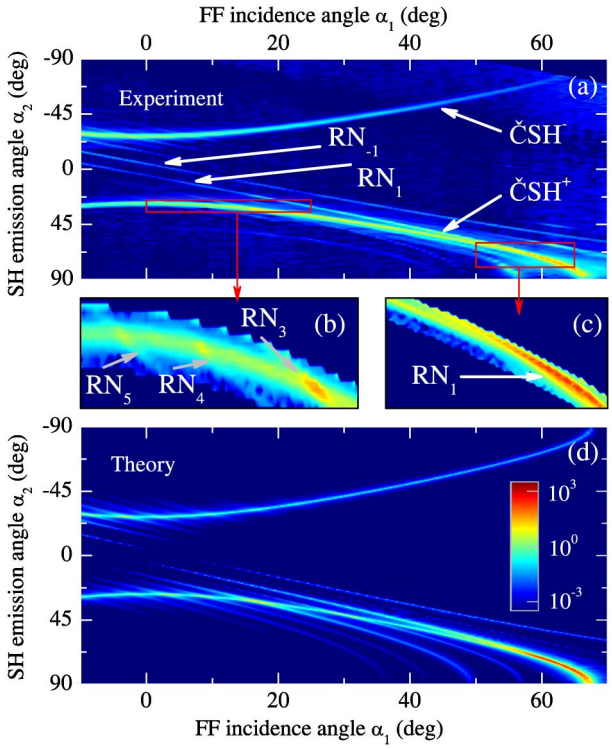

Fig. 3. (Color online) (a) Experimentally measured SH enhancement η as a function of FF incidence angle α_1 and external SH emission angle α_2. (b) and (c) detailed scan around points where Čerenkov emission curve crosses Raman–Nath emission curves ($m = 1, 3, 4, 5$). (d) Numerically calculated SH enhancement map (see text for details). Color coding is the same on all maps.

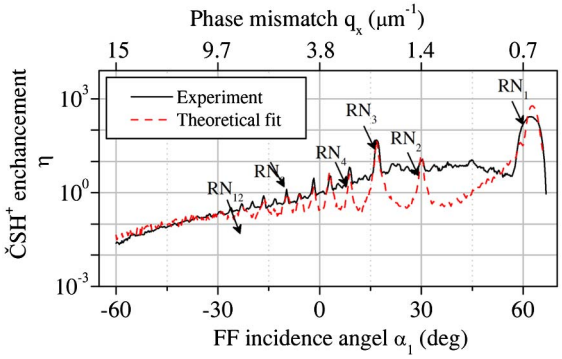

Fig. 4. (Color online) Measured (solid line) and theoretical fit (dashed line) ČSH$^+$ enhancement.

lines of the Raman–Nath process. These crossing points represent the previously discussed exact nonlinear Bragg scattering conditions. Figure 3(d) is a theoretical counterpart of Fig. 3(a) calculated according to Eq. (1), where NLPC parameters were obtained from theoretical fit to experimental data. In Fig. 4, the solid line shows the measured ČSH$^+$ enhancement η as a function of the FF incidence angle α_1. The RN resonances originating from RN_1 up to RN_{12} are clearly visible. Note that apart from expected odd orders (in the case of duty cycle 50%, only odd Fourier components are nonzero), the even (weaker) orders are also visible, which is a clear evidence of imperfect poling. The nonlinear Bragg matching using the primary RLV G_1 leads to the maximum enhancement of $\eta = 271$. The dashed line represents theoretically calculated ČSH$^+$ enhancement averaged over 50 realizations of domain structure. We considered an NLPC consisting of 50 domains with their widths exhibiting gamma distribution. The parameters—poling period $\Lambda = 9.25\,\mu$m, dispersion $\sigma = 0.49\ \mu$m, and duty cycle 46%—were found by fitting the theoretical results to the experimental data. A very good correspondence between theory and experiment for ČSH was achieved [compare Figs. 3(a) and 3(d)].

In conclusion, we demonstrated significant (over 10^2) enhancement of the ČSHG in periodically poled nonlinear crystal by varying the angle of incidence of the fundamental wave. We showed that this effect is caused by the simultaneous fulfillment of the Čerenkov and Raman–Nath emission conditions leading to the perfect nonlinear Bragg diffraction regime. Our experimental results are in excellent agreement with theory.

This work was supported by the Australian Research Council. P. Roedig gratefully acknowledges financial support of the Deutscher Akademischer Austauschdienst (DAAD) and the Center for Nonlinear Science (CeNoS).

References

1. S. Saltiel, Y. Sheng, N. Voloch-Bloch, D. Neshev, W. Krolikowski, A. Arie, K. Koynov, and Y. Kivshar, IEEE J. Quantum Electron. **45**, 1465 (2009).
2. S. M. Saltiel, D. N. Neshev, R. Fischer, W. Krolikowski, A. Arie, and Y. S. Kivshar, Phys. Rev. Lett. **100**, 103902 (2008).
3. P. Molina, M. O. Ramírez, B. J. García, and L. E. Bausá, Appl. Phys. Lett. **96**, 261111 (2010).
4. M. Ayoub, P. Roedig, J. Imbrock, and C. Denz, Opt. Lett. **36**, 4371 (2011).
5. Y. Sheng, W. Wang, R. Shiloh, V. Roppo, Y. Kong, A. Arie, and W. Krolikowski, Appl. Phys. Lett. **98**, 241114 (2011).
6. Y. Sheng, A. Best, H.-J. Butt, W. Krolikowski, A. Arie, and K. Koynov, Opt. Express **18**, 16539 (2010).
7. S. M. Saltiel, D. N. Neshev, W. Krolikowski, A. Arie, O. Bang, and Y. S. Kivshar, Opt. Lett. **34**, 848 (2009).
8. Y. Sheng, V. Roppo, Q. Kong, K. Kalinowski, Q. Wang, C. Cojocaru, J. Trull, and W. Krolikowski, Opt. Lett. **36**, 2593 (2011).
9. K. Kalinowski, Q. Kong, V. Roppo, A. Arie, Y. Sheng, and W. Krolikowski, Appl. Phys. Lett. **99**, 181128 (2011).
10. Y. Sheng, Q. Kong, V. Roppo, K. Kalinowski, C. C. Qi Wang, and W. Krolikowski, J. Opt. Soc. Am. B **29**, 312 (2012).
11. T. Ellenbogen and A. Arie, Opt. Commun. **277**, 423 (2007).
12. A. Shapira and A. Arie, Opt. Lett. **36**, 1933 (2011).
13. X. Deng, H. Ren, H. Lao, and X. Chen, Appl. Phys. B **100**, 755 (2010).
14. H. Ren, X. Deng, and X. Chen, arXiv:1010.1593v1 (2010).
15. S. Russell, P. Powers, M. Missey, and K. Schepler, IEEE J. Quantum Electron. **37**, 877 (2001).
16. Y. L. Grand, D. Rouede, C. Odin, R. Aubry, and S. Mattauch, Opt. Commun. **200**, 249 (2001).
17. M. Fejer, G. Magel, D. Jundt, and R. Byer, IEEE J. Quantum Electron. **28**, 2631 (1992).